

Article

# Externally Heated Hollow Cathode Arc Plasma Source for Experiments in Plasma Wakefield Acceleration

Ryan Roussel <sup>1,\*</sup>, Gerard Andonian <sup>1</sup>, Claire Hansel <sup>1</sup>, Gerard Lawler <sup>1</sup>, Walter Lynn <sup>1</sup>, Nathan Majernik <sup>1</sup>, River Robles <sup>1</sup>, Kunal Sanwalka <sup>1</sup> , Eric Wisniewski <sup>2</sup> and James Rosenzweig <sup>1</sup>

<sup>1</sup> Particle Beam Physics Laboratory, University of California Los Angeles, Los Angeles, CA 90095, USA

<sup>2</sup> Argonne Wakefield Accelerator, Argonne National Laboratory, Lemont, IL 60439, USA

\* Correspondence: roussel@ucla.edu

Received: 31 July 2019; Accepted: 5 September 2019; Published: 10 September 2019



**Abstract:** An externally heated, hollow cathode arc source was recommissioned at UCLA for use in experiments to drive plasma wakefields with shaped beams at the Argonne Wakefield Accelerator. The hollow cathode arc source provides a robust plasma column with a density in the  $10^{13}$ – $10^{14}$   $\text{cm}^{-3}$  range while external heating of the cathode allows the plasma arc regime to be accessed with applied voltages down to 20 V. Overall source operating principals are described, along with time-resolved plasma current measurements and plasma density characterization with the use of a triple Langmuir probe. The results show that relevant plasma densities that match facility beam parameters are readily achievable.

**Keywords:** plasma wakefield acceleration; hollow cathode arc; discharge

## 1. Introduction

The Argonne Wakefield Accelerator (AWA) facility at Argonne National Laboratory provides a unique platform for measuring wakefield dynamics of both dielectric and plasma-based wakefield structures. Previous experiments using the emittance exchange (EEX) beamline [1] at AWA have studied high transformer ratio wakefield generation using longitudinally ramped beams in dielectric structures [2]. Here we discuss recommissioning of a hollow cathode arc (HCA) plasma source at UCLA for use in plasma wakefield experiments at AWA, including high transformer ratio and flat beam propagation experiments.

High transformer ratio experiments at AWA aim to generate wakefields with a transformer ratio greater than the classical limit for symmetric beams  $\mathcal{R} < 2$ , using longitudinally asymmetric beams generated by emittance exchange [3]. The transformer ratio from a linearly ramped drive beam is given by  $\mathcal{R} = \pi l / \lambda_p$  where  $l$  is the length of the drive and  $\lambda_p$  is the plasma wavelength [4]. Longitudinally ramped beams generated by emittance exchange at AWA are nominally  $\sim 20$  ps (6 mm) long, so to achieve high transformer ratios with a drive length  $l = 2\lambda_p$  a plasma density target of  $n_p \approx 1.2 \times 10^{14}$   $\text{cm}^{-3}$  was set for the HCA source.

## 2. Hollow Cathode Arc Plasma Source and Characterization

Hollow cathode arc plasma sources have been theoretically and experimentally investigated as a robust method of argon plasma production in the  $10^{12}$ – $10^{14}$   $\text{cm}^{-3}$  range [5]. In contrast to planar electrode plasma sources, the HCA cathode is made of a hollow tube as seen in Figure 1. The UCLA plasma source uses a set of concentric tantalum tubes with diameters of 8 and 10 mm to form the hollow cathode. This feature allows the plasma to extend inside the cathode, significantly increasing the active cathode surface area. Furthermore, emitted electrons from the inner tube surface and liberated

electrons from ionization events inside the cathode have an increased probability of colliding with neutral gas particles due to this geometry. Combining a hollow cathode with a ring anode also allows for collinear propagation of a beam with the plasma column axis while also reducing beam exposure to neutral particles. The ring anode has a similar inner diameter and was placed between 6–8 cm from the cathode edge to optimize plasma density profile.

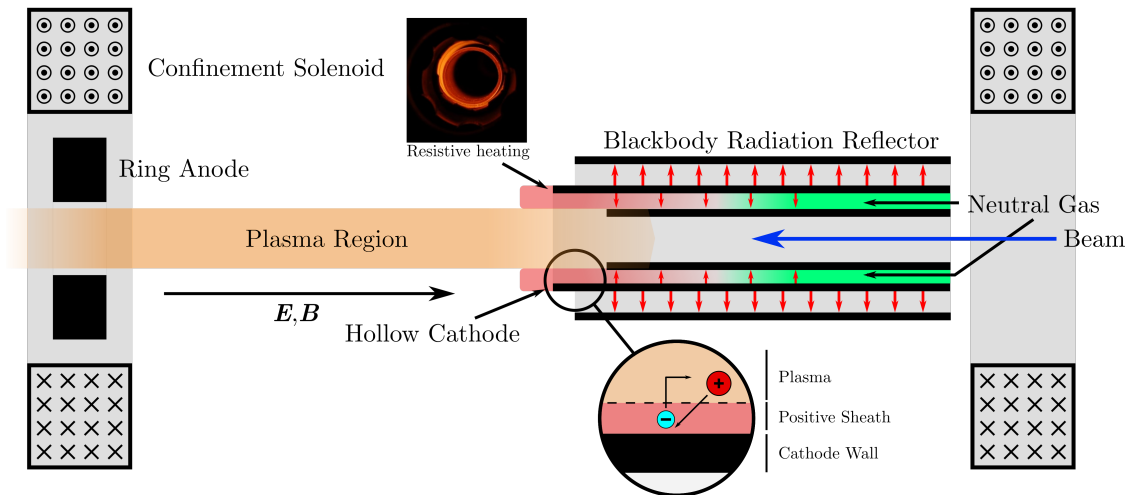


**Figure 1.** Cross section of the hollow cathode arc plasma source showing active regions of the discharge.

A unique aspect of the UCLA plasma source is external heating of the cathode walls, which allows access to the arc discharge regime at extremely low voltages. Without external heating, the plasma arc regime is reached only after thermionic electron emission, due to localized heating by plasma ion bombardment [6]. In the UCLA plasma source, the cathode tube is resistively heated using a high current ( $\sim 1000$  A) to roughly 2000 K before discharges are triggered. A tantalum shield outside the heated cathode reflects blackbody radiation to maintain the extremely high temperature. At this temperature, thermionic electron emission is significant source of primary electrons  $\sim 3$  mA [7], which when accelerated by a discharge voltage, trigger Townsend avalanches in the inter-electrode space. This circumvents voltage requirements for establishing self-sustaining plasmas, allowing the discharge to reach arc level currents ( $>1$  A) in low pressure plasmas at low breakdown voltages, as seen in Figure 2a.

Figure 2a shows a measurement of the modified Paschen curve [8] due to external cathode heating. Minimum distance between the ring anode face and the cathode face was set to be 8 cm. For each chamber pressure  $p$ , the voltage increased from 0 V until a discharge with current of at least 1 A developed for 10 consecutive shots. This voltage was then considered to be the upper limit for breakdown voltage  $V_B$  for a given chamber pressure. It is reasonable to assume that small errors in the breakdown voltage measurement of up to a few volts, due to the rapid transition from glow to arc regimes. The measured dependence of breakdown on  $pd$  shows differences in structure when compared to theoretical predictions [8]. The extremely low minimum discharge voltage and a lack of asymptotic behavior at low gas pressures is particularly significant, due to constant thermionic electron emission.

Figure 2b shows temporal evolution of the plasma discharge current as a function of applied voltage. Each curve represents a close approximation to the average current profile at a given voltage as shot to shot variations of the current varied by less than 5%. We observe that at low voltages the discharge current reaches a peak significantly after the voltage is applied (orange line). This delay is often referred to as the primary formative time lag  $\tau_p$  of the plasma discharge, and is influenced by the “overvoltage” applied  $V_o = V - V_B$ . If the voltage applied is precisely equal to the breakdown,  $V_o = 0$  and the formative time  $\tau \rightarrow \infty$ . As overvoltage increases, the time lag decreases in an exponential manner, consistent with similar experiments [6].

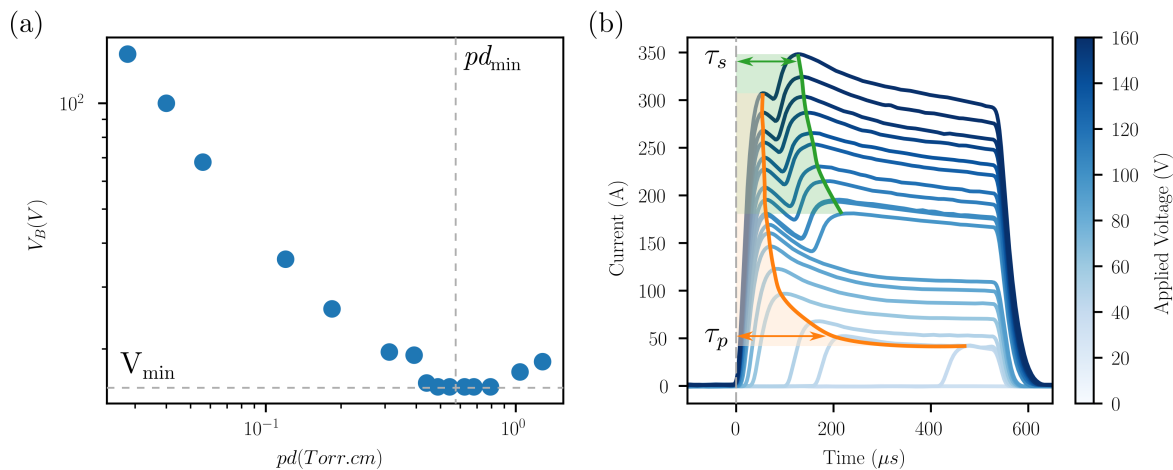


**Figure 2.** Plasma discharge measurements with external heating at 5 kW and solenoid current of 10 A. (a) Curve of plasma breakdown voltages  $V_B$  where  $I > 1$  A. Minimum breakdown voltage is 15.6 V at a pressure of  $p = 7.8 \times 10^{-2}$  Torr ( $d = 8$  cm). (b) Current traces of discharges at different applied voltages. Voltage pulse is applied  $0 < t < 600 \mu\text{s}$  and  $\tau_p, \tau_s$  are the primary and secondary formative time lags for reaching steady state discharge.

A secondary peak in the discharge current is observed once a voltage of  $\approx 80$  V is applied. This secondary electron emission mechanism is attributed to cathode emission from positive-ion impact. Plasma ions are accelerated towards the cathode by the applied field. Once ion kinetic energy is sufficient, impact from these particles onto the cathode surface triggers secondary electron emission. Formative time lag for this secondary process  $\tau_s \gg \tau_p$  is longer due to relatively low ion drift velocity.

The longitudinal plasma density was characterized using a triple Langmuir probe [9]. This diagnostic uses three tungsten probes (seen in Figure 3) to simultaneously measure three locations on the plasma I-V curve to determine the density. As seen in Figure 3b,d two of the probes are biased to one another to sample the ion and electron saturation currents respectively. Net current is measured using a  $100 \Omega$  shunt resistor ( $I_{sat} \sim 1$  mA). The third probe is isolated from the others and is used to measure the plasma floating voltage Figure 3c. If  $V_{bias}$  is selected such that  $eV_{d1} = e(V_{bias} + I_{sat}R) \gg k_b T_e$  where  $T_e$  is the electron temperature, the  $V_-$  probe is guaranteed to be in the ion saturation regime and  $k_b T_e = \ln(2)eV_{d2}$ . The plasma electron density can then be calculated via a simultaneous measurement of  $V_{d2}$  and saturation current. The plasma density is given by [9]

$$n_e = 1.05 \times 10^9 M^{1/2} S^{-1} I T_e^{-1/2} [\exp(eV_{d2}/k_b T_e) - 1]^{-1} \tag{1}$$

where  $M$  is the effective atomic or molecular weight of the ions,  $S$  is the surface area of the exposed probe in  $\text{mm}^2$ ,  $I$  is the measured current in  $\mu\text{A}$  and the plasma density is given in  $\text{cm}^{-3}$ . Systematic errors in this measurement technique result from nonuniform ion saturation current as a function of voltage. It has been estimated that the error in plasma density measurements for most systems using this method ranges from 10–25% [9].

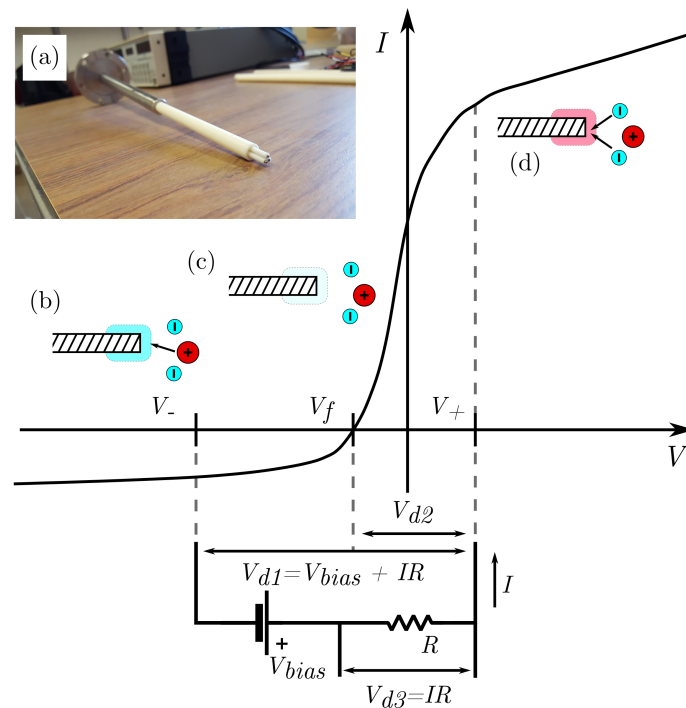


**Figure 3.** Overview of triple Langmuir probe direct display plasma density measurement. Three electrodes (a) are inserted into the plasma region. Two of the probes are biased with respect to one another using  $V_{bias}$  to collect ion saturation current at  $V_-$  (b) and electron saturation current at  $V_+$  (d) where  $V_+ - V_- = V_{d1}$ . The final probe (c) is left at the plasma floating potential  $V_f$  where no net current is collected. A simultaneous measurement of the potential difference  $V_{d2} = V_+ - V_f$  and the current through the biased probes (measured using shunt resistor voltage difference  $V_{d3}$ ) yields a measurement of the plasma density.

The triple Langmuir probe was mounted on a linear stage to map out the on-axis plasma density inside and outside the inter-electrode region. The plasma profile was measured using a bias voltage of  $V_{bias} = 67$  V for three different solenoid settings relevant for beam-plasma experiments and at a chamber pressure of 50 mTorr (Figure 4). It was observed that shot to shot differences in the measured plasma density was lower than predicted systematic errors. Our measurement shows that plasma density increases with increasing solenoid current which is consistent with a decrease in the electron gyroradius as a function of magnetic field strength  $r_g \propto 1/B$ , and matches results from previous experiments [5]. If the solenoid current increases further, discharges eventually become suppressed at a given cathode tube temperature. Constriction of the external (inter-electrode region) and internal (inside the hollow cathode) plasma columns increases the required voltage for discharge [5]. Once the tubes are heated further, discharges resume with a higher density, due to the increase in thermionic current causing an increase in ionization fraction (from  $< 3\%$  to  $\sim 10\%$ ). Further increases in temperature will continue to increase the ionization fraction; however it is limited by cathode damage concerns, as it was found that above roughly 2000 K the cathode tube can deform and interrupt the heating circuit.

Due to engineering constraints, the triple Langmuir probe transverse size was comparable to the radius of the outer hollow cathode tube. Once the probe traveled far into the inter-electrode space it started to disrupt the plasma discharges. This is demonstrated by an unexpected drop in density for the last few points in Figure 4 after which the source stopped discharging. We hypothesize that inserting the probe beyond a certain limit disrupts gas flow or discharge path between the two electrodes, resulting in a measured drop in density and eventually the complete suppression of discharges.

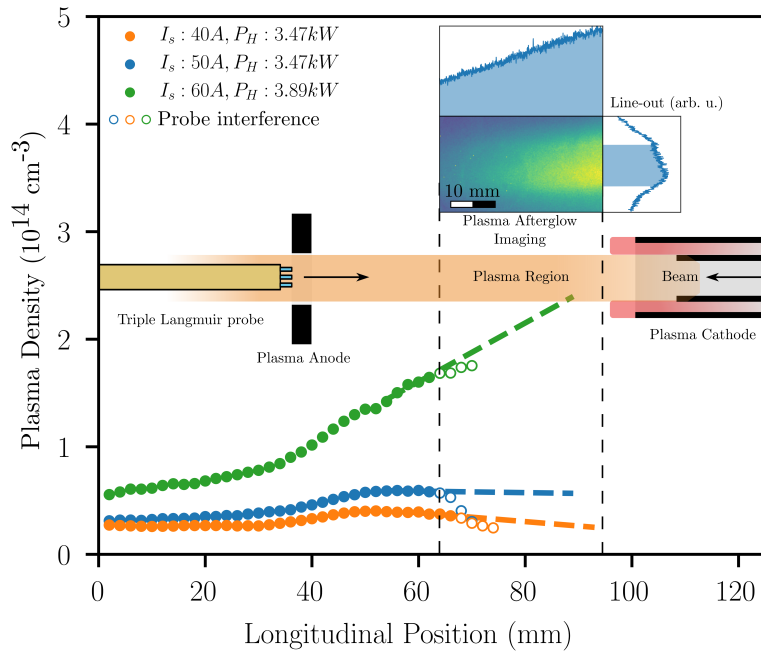


**Figure 4.** Longitudinal plasma density profile characterization as a function of solenoid current  $I_s$  and heating power delivered to cathode tubes  $P_H$  with a cartoon of source geometry and diagnostics properly scaled in the longitudinal direction. Hollow points represent measurements affected by probe interference in the plasma discharge. The unaffected profile is extrapolated (dashed lines) using a linear relation, inferred from a measurement of the corresponding plasma afterglow brightness (inset). Imaging also shows a root-mean-squared plasma column width of 8 mm.

To characterize this region, we used direct imaging of the optical plasma afterglow using a CCD camera. Since light emission from heating the cathode prevents detailed imaging inside of the plasma source, the CCD was electronically gated to a pulse length of 20  $\mu\text{s}$  and was triggered simultaneously with the plasma discharge. This technique allows capture of the instantaneous light from arc discharge, which is considerably brighter than the background blackbody radiation during the gated period. Assuming the light emission intensity is proportional to the plasma density [10] a projection of the CCD image intensity onto the longitudinal axis is used to extrapolate the absolute plasma density from the last points before the probe starts to suppress the discharge. This extrapolation is denoted by the dashed lines in Figure 4 and uses points before the fall off in plasma density due to probe interference. Furthermore, the technique corroborates that the transverse extent of the plasma is roughly equal to the hollow cathode diameter. Imaging the plasma profile at the exit or inside of the hollow cathode is not accessible. Based on the estimates of the gas density in this region, the plasma density is at its highest just inside the cathode, then drops quickly to zero at the smaller tube end, where gas density drops to zero.

We can characterize these plasma profiles by calculating their effective length  $L_{eff}$  and the mean plasma density  $\langle n_p \rangle$  as

$$L_{eff} = \frac{1}{n_{p,max}} \int_{z_{min}}^{z_{max}} n_p(z') dz' \quad (2a)$$

$$\langle n_p \rangle = \frac{1}{z_{max} - z_{min}} \int_{z_{min}}^{z_{max}} n_p(z') dz' \quad (2b)$$

For a zero-order calculation we assume a linear plasma ramp from the end of the extrapolation (at  $z = 95$  mm) region to the end of the inner cathode tube (at  $z = 110$  mm). Based on this assumption,

the calculated effective length and average plasma density for the three profiles in Figure 4 are shown in Table 1.

**Table 1.** Calculated plasma stats for profiles in Figure 4.

Solenoid Current (A)	Heater Power (kW)	$L_{eff}$ (mm)	$\langle n_p \rangle$ ( $10^{14} \text{ cm}^{-3}$ )
40	3.47	76	0.3
50	3.47	76	0.4
60	3.89	57	1.3

Taking into account our assumptions about the plasma profile and the measurement systematics we predict variations in the effective plasma column length and average plasma density up to  $\sim 25\%$ .

From these metrics we recover that an increase in solenoid field increases the plasma density as predicted [5]. Furthermore, our data suggests that an increase in tube temperature due to increased heater power also gives rise to an increase in plasma density. It is likely that an increase in thermal electron current from the heated cathode leads to a higher ionization fraction, as the plasma density increases without an increase in gas pressure or flow rate. Finally, the maximum average plasma density matches well with the AWA drive beam parameters.

### 3. Conclusions

This paper describes the hollow cathode arc plasma source developed at UCLA, which is used for plasma wakefield acceleration measurements at the Argonne Wakefield Accelerator. Plasma discharge arc characteristics were measured across different chamber pressures and with varying applied voltages. The plasma density profile was measured using a triple Langmuir probe in conjunction with measurements of the optical plasma afterglow. The reported measurements demonstrate that the plasma density profiles, with density in the range of  $0.3\text{--}1.3 \times 10^{14} \text{ cm}^{-3}$  from the HCA source, are suitable for longitudinally shaped bunch wakefield experiments to investigate high transformer ratios.

**Author Contributions:** Conceptualization, R.R. (Ryan Roussel), G.A. and J.R.; methodology, R.R. (Ryan Roussel), G.A., K.S., G.L., W.L., N.M.; software, R.R. (Ryan Roussel), R.R. (River Robles), C.H.; validation, R.R. (Ryan Roussel), G.A. and J.R.; formal analysis, R.R. (Ryan Roussel); investigation, R.R. (Ryan Roussel), E.W.; resources, G.A., J.R.; data curation, R.R. (Ryan Roussel); writing—original draft preparation, R.R. (Ryan Roussel); writing—review and editing, G.A., J.R.; visualization, R.R. (Ryan Roussel); supervision, G.A.; project administration, G.A.; funding acquisition, G.A., J.R.

**Funding:** This research was funded by the DOE under contract number DE-SC0017648.

**Acknowledgments:** The author would like to thank Oliver Williams and Atsushi Fukasawa for their technical assistance during the commissioning process.

**Conflicts of Interest:** The authors declare no conflict of interest.

### References

- Ha, G.; Cho, M.; Namkung, W.; Power, J.; Doran, D.; Wisniewski, E.; Conde, M.; Gai, W.; Liu, W.; Whiteford, C.; et al. Precision Control of the Electron Longitudinal Bunch Shape Using an Emittance-Exchange Beam Line. *Phys. Rev. Lett.* **2017**, *118*, 104801. [[CrossRef](#)] [[PubMed](#)]
- Gao, Q.; Ha, G.; Jing, C.; Antipov, S.; Power, J.; Conde, M.; Gai, W.; Chen, H.; Shi, J.; Wisniewski, E.; et al. Observation of High Transformer Ratio of Shaped Bunch Generated by an Emittance-Exchange Beam Line. *Phys. Rev. Lett.* **2018**, *120*, 114801. [[CrossRef](#)] [[PubMed](#)]
- Bane, K.L.F.; Wilson, P.B.; Weiland, T. Wake fields and wake field acceleration. In *AIP Conference Proceedings*; AIP: College Park, MD, USA, 1985; Volume 127, pp. 875–928.
- Bane, K.L.F.; Chen, P.; Wilson, P.B. On Collinear Wake Field Acceleration. *IEEE Trans. Nucl. Sci.* **1985**, *32*, 3524–3526. [[CrossRef](#)]

5. Delcroix, J.L.; Trindade, A.R. Hollow Cathode Arcs. In *Advances in Electronics and Electron Physics*; Marton, L., Ed.; Academic Press: Cambridge, MA, USA, 1974; Volume 35, pp. 87–190.
6. Nasser, E. *Fundamentals of Gaseous Ionization and Plasma Electronics*; Wiley-Interscience: Hoboken, NJ, USA, 1971.
7. Richardson, O.W. *Thermionic Emission from Hot Bodies*; Watchmaker Publishing: Seaside, OR, USA, 2003.
8. Paschen, F. Ueber die zum Funkenübergang in Luft, Wasserstoff und Kohlensäure bei verschiedenen Drucken erforderliche Potentialdifferenz. *Annalen der Physik* **1889**, *273*, 69–96. [[CrossRef](#)]
9. Chen, S.; Sekiguchi, T. Instantaneous Direct Display System of Plasma Parameters by Means of Triple Probe. *J. Appl. Phys.* **1965**, *36*, 2363–2375. [[CrossRef](#)]
10. Chaplin, V.H.; Bellan, P.M. Emission and afterglow properties of an expanding RF plasma with nonuniform neutral gas density. *Phys. Plasmas* **2016**, *23*, 083506. [[CrossRef](#)]



© 2019 by the authors. Licensee MDPI, Basel, Switzerland. This article is an open access article distributed under the terms and conditions of the Creative Commons Attribution (CC BY) license (<http://creativecommons.org/licenses/by/4.0/>).